Research Square

Preprints are preliminary reports that have not undergone peer review.
They should not be considered conclusive, used to inform clinical practice,
or referenced by the media as validated information.

Uncertainty in climate sensitivity links to Antarctic sea ice

Olivia Linke

olivia.linke@misu.su.se

Stockholm University https://orcid.org/0000-0002-5286-2185

Luna Suau

Paris-Saclay University

Noel Chawang

Karlsruhe Institute of Technology (KIT) https://orcid.org/0000-0003-3768-7996

Peter Churchill

Stockholm University

Vårin Sørensen

University of Oslo

Julien Lenhardt

Swedish Meteorological and Hydrological Institute (SMHI) https://orcid.org/0000-0002-9949-3989

Rodrigo Caballero

Stockholm University

Thorsten Mauritsen

Stockholm University https://orcid.org/0000-0003-1418-4077

Annica Ekman

Stockholm University

Article

Keywords: Climate sensitivity, Antarctic sea ice, Southern Ocean bias, Climate feedbacks, SST pattern, CMIP6

Posted Date: June 9th, 2026

DOI: https://doi.org/10.21203/rs.3.rs-9948407/v1

License: This work is licensed under a Creative Commons Attribution 4.0 International License.
Read Full License

Additional Declarations: There is **NO** Competing Interest.

Uncertainty in climate sensitivity links to Antarctic sea ice

Olivia Linke[1*], Luna Suau[2], Noel M. Chawang[3], Peter L. Churchill[4], Vårin F. Sørensen[5], Julien Lenhardt[6], Rodrigo Caballero[1], Thorsten Mauritsen[1], Annica M. L. Ekman[1]

[1]Department of Meteorology and Bolin Centre for Climate Research, Stockholm University, Stockholm, Sweden.
[2]Physics Department, École Normale Supérieure Paris-Saclay, Paris-Saclay University, Gif-sur-Yvette, France.
[3]Institute of Meteorology and Climate Research Troposphere Research, Karlsruhe Institute of Technology (KIT), Karlsruhe, Germany.
[4]Department of Environmental Science and Bolin Centre for Climate Research, Stockholm University, Stockholm, Sweden.
[5]Department of Geosciences, University of Oslo, Oslo, Norway.
[6]Rossby Centre, Swedish Meteorological and Hydrological Institute (SMHI), Norrköping, Sweden.

*Corresponding author(s). E-mail(s): olivia.linke@misu.su.se;

Abstract

Climate sensitivity is a key metric for future global warming projections under continued greenhouse-gas emissions, yet Earth system models (ESMs) exhibit a wide uncertainty in its magnitude. We show that the inter-model spread in effective climate sensitivity (ECS) is systematically linked to the spread in pre-industrial Antarctic sea ice area (SIA). Models with larger pre-industrial Antarctic SIA project less stabilizing global feedback through (1) preconditioning stronger sea ice loss and larger surface albedo feedback in the Southern Ocean, and (2) exhibiting distinct hemispheric patterns of sea surface temperature (SST) warming associated with larger shortwave cloud feedback beyond high latitudes. Notably, the dominant mode of SST pattern variability across ESMs resembles Southern Ocean–tropical teleconnection pathways previously identified in idealized perturbation studies. Here, fingerprints of these structures emerge across coupled ESMs, with strong links to Antarctic sea ice. We thus show that a substantial fraction of hemispheric feedback uncertainty is rooted in Southern Ocean

mean-state biases of ESMs, prior to external forcing. Using Antarctic SIA as a proxy in conjunction with satellite observations, we construct a process-oriented emergent constraint on ECS that yields a very likely (90%) range of 3.3–5.0 K, placing it toward the upper end of the latest IPCC estimate.

Keywords: Climate sensitivity, Antarctic sea ice, Southern Ocean bias, Climate feedbacks, SST pattern, CMIP6

Introduction

How strongly the Earth warms in response to external forcing is governed by climate feedbacks. As the planet warms, changes in temperature, surface albedo, water vapour, and clouds alter the top-of-atmosphere energy balance, collectively determining the additional warming required to restore equilibrium [1–4]. The net feedback thus sets the equilibrium climate sensitivity, the global mean surface temperature increase required to balance a doubling of CO_2. In practice, climate sensitivity is commonly estimated in Earth system models (ESMs) using the regression method applied to benchmark experiments of CO_2-quadrupling, which yields the effective climate sensitivity (hereafter ECS; [4–8]). Although ECS reflects centennial-scale adjustments and may differ from the "true" equilibrium state realized over millennia [9], it remains a widely used measure of the Earth's response to a given greenhouse gas forcing [4, 5, 10].

Despite decades of progress, successive generations of ESMs continue to exhibit substantial uncertainty in ECS. The latest generation of models from the Coupled Model Intercomparison Project Phase 6 (CMIP6) shows a wider spread and a more pronounced high-sensitivity tail than its predecessor, CMIP5 [8, 10, 11]. The increase in ECS in a substantial fraction of CMIP6 models has been attributed to an increased shortwave feedback, primarily owed to a larger low-cloud feedback in the extratropics [8]. At the same time, changes in mean-state cloud properties between model generations may also have influenced Antarctic sea ice, contributing on average to larger pre-industrial sea ice extent and stronger subsequent ice loss under CO_2 forcing in CMIP6 compared to CMIP5 [11]. These changes have been hypothesized to contribute to the elevated shortwave feedback in CMIP6 through an enhanced Southern Ocean surface albedo feedback [11]. Yet the extent to which inter-model differences in Antarctic sea ice contribute to feedback and ECS uncertainty has not been systematically assessed.

In addition, the impacts of Southern Ocean sea ice loss and warming are unlikely to remain confined to high latitudes, but may modulate remote feedback responses across the Southern Hemisphere. Previous model perturbation experiments have suggested that the sustained Southern Ocean cooling and sea ice expansion observed during the satellite era generated negative remote cloud feedback anomalies by altering hemispheric patterns of sea surface temperature (SST) through atmospheric and oceanic teleconnections [12, 13]. Although ESMs struggle to reproduce the observed Southern Ocean SST and sea ice trends [13–17], these studies highlight the potential for Southern Ocean variability to mediate feedback responses well beyond high latitudes

[12, 13, 18–20]. While those cross-latitude couplings are established in atmosphere-only experiments through systematically perturbing Southern Ocean climate [12, 13], it remains unclear whether such links emerge consistently across an ensemble of freely evolving coupled ESMs.

Here we propose that the substantial uncertainty in Antarctic mean-state sea ice area (SIA) in CMIP6 [21] contributes to the spread in ECS. We show that ESMs with larger pre-industrial (*piControl*) Antarctic SIA systematically exhibit stronger global feedback through (1) a more positive Southern Ocean surface albedo feedback, and (2) a larger extra-polar shortwave cloud feedback associated with distinct SST warming patterns over the Southern Hemisphere. Leveraging these relationships across ESMs, we construct a process-oriented emergent constraint based on the observed Antarctic SIA climatology. While Antarctic SIA is not the sole determinant of climate sensitivity, we propose it as a proxy of the coupled Southern Hemisphere mean state, which partly sets the stage for the subsequent evolution of long-term climate feedbacks and ECS.

Results

Global feedback links to pre-industrial Antarctic SIA

In Figure 1 we examine relationships between pre-industrial Antarctic SIA, its response to CO_2 forcing, and global net feedback across CMIP6 models. Figure 1a shows the annual-mean sea ice edge in the pre-industrial control climate, colour-coded by global feedback strength. For a substantial fraction of models, the pre-industrial sea ice edge lies poleward of the observed climatology 1979–2014, which marks a time period of rather stable Antarctic SIA with weakly positive trends [22, 23]. Our results are consistent with the low-SIA bias identified in the historical mean state 1979–2014 for CMIP6 [21], and further connects to a long-standing issue in climate modelling: the persistent Southern Ocean warm-SST bias, which has persisted across multiple generations of ESMs [24, 25].

Strikingly, models with unrealistically small initial SIA tend to show the most negative global feedbacks. Conversely, CMIP6 models with a more equatorward sea ice edge, closer to the observed climatology, exhibit less negative global feedbacks (Fig. 1a). Thus, the observed climatological sea ice edge is better captured by models with larger pre-industrial SIA. These large-SIA models project a higher sensitivity of sea ice melt to global warming $\Delta\text{SIA}/\Delta\overline{T}$, and larger absolute sea ice loss ΔSIA over the course of the CO_2-forcing experiment (Fig. 1b,c). In turn, larger sea ice loss is associated with less stabilizing global feedbacks across ESMs (Fig. 1d). Taken together, these relationships across ESMs indicate that the pre-industrial sea ice mean state largely preconditions the trajectory of subsequent ice loss, and thus partly constrains the coupled evolution of sea ice and long-term feedback.

Accordingly, pre-industrial SIA is correlated with global feedback across ESMs (Fig. 1e), implying that part of the feedback uncertainty is rooted in the baseline climate. The same cannot be concluded for the Arctic, where uncertainty in mean-state SIA is substantially smaller [21], and no noteworthy correlation arises between pre-industrial SIA, and subsequent sea ice loss and global feedback (Fig. A1). This reinforces our hypothesis that it is primarily biases in the Southern Ocean mean state

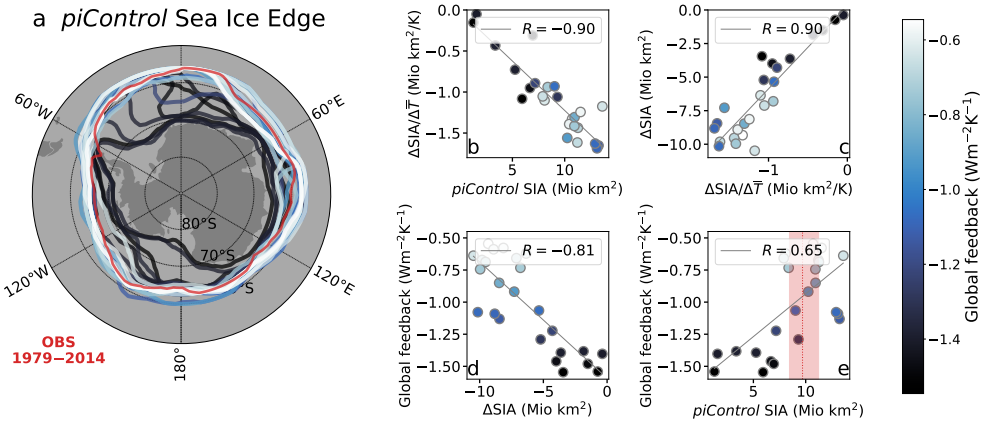


Fig. 1 Antarctic sea ice and global feedback across CMIP6 models. (a) Mean-state Southern Hemisphere sea ice edge in *piControl*, colour coded by global feedback in CO_2-quadrupling simulations. OBS: Observed climatological sea ice edge 1979–2014 from three satellite products (OSI SAF, NASA Team, Bootstrap). Inter-model scatter plots show linear relationships between (b) *piControl* Antarctic SIA and sea ice melt sensitivity $\Delta SIA/\Delta\overline{T}$, (c) $\Delta SIA/\Delta\overline{T}$ and absolute sea ice loss ΔSIA, and (d) ΔSIA and global feedback. (e) Connecting (b)–(d): *piControl* Antarctic SIA and global feedback. Red shading: Observed climatological SIA, with uncertainty range derived as minimum to maximum annual value over 1979–2014 and three data records. All linear relationships show Pearson's correlation coefficient R, and are significant at the 95% confidence level.

prior to external forcing that set the stage for important feedback responses with global-scale impact.

A growing body of previous work has identified potential causes for the lingering Southern Ocean sea ice bias in ESMs, including atmospheric processes and atmosphere–ocean–sea-ice coupling mechanisms (summarized in ref. [23]). However, no consensus is reached regarding their relative contributions. Here, we do not seek to resolve the origins of the bias itself, but rather to place uncertainties tied to the Southern Ocean mean state into the broader context of a long-standing challenge in climate science: identifying key regions and processes that govern persistent uncertainty in ECS.

Next, we show that the connection between Antarctic sea ice and global feedback primarily occurs through Southern Hemisphere shortwave feedbacks. Figure 2 shows zonal-mean feedbacks across models, colour-coded by Antarctic sea ice loss. The net shortwave feedback is decomposed into cloud and surface albedo components, with highlighted regions indicating robust linear correlations between Antarctic sea ice loss and local feedback strength.

Figure 2a shows that three latitude bands exhibit robust relationships, where models with larger Antarctic sea ice loss tend to exhibit a larger net feedback (indicated by negative correlation coefficients). Over the Southern Ocean south of ∼60°S, greater sea ice loss is associated with a more positive shortwave feedback owed to a larger surface albedo feedback (Fig. 2b,d). In the Southern mid-latitudes, models with larger sea ice loss exhibit a larger shortwave feedback due to a more positive shortwave cloud

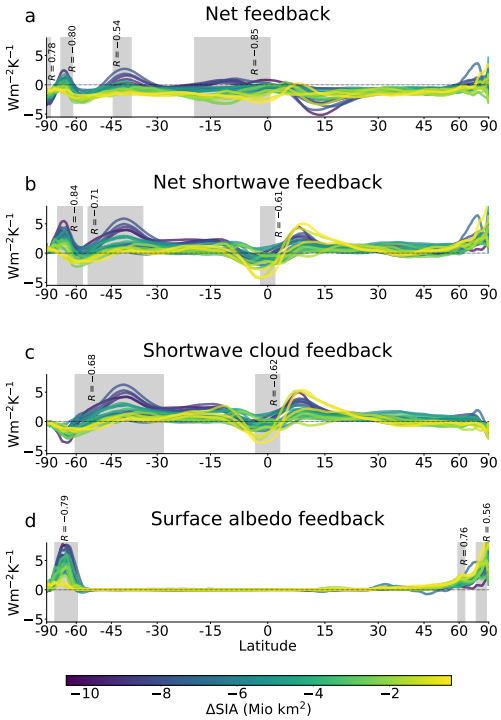


Fig. 2 Links between Antarctic sea ice loss and zonal feedbacks across CMIP6 models. Zonal-mean net and shortwave feedbacks show individual ESMs colour-coded by the magnitude of Antarctic sea ice loss ΔSIA. Grey shadings: Latitude bands where the relationship between ΔSIA and local feedback strengh is statistically robust. Robustness is indicated where regression slopes exceed the 75th percentile of absolute slopes across latitudes, and regressions are significant at the 95% confidence level. Numbers indicate the maximum linear correlation coefficient R within each latitude band.

feedback (Fig. 2b,c). Likewise, a narrower band of robust correlation appears around the equator, where larger Antarctic sea ice loss coincides with a larger net shortwave and cloud feedback. Here, the signal is further amplified in the net feedback through contributions from the longwave cloud feedback (Fig. B2a,b).

In contrast, over the Antarctic continent, greater sea ice loss is associated with more negative net feedback (positive correlation in Fig. 2a). This relationship is driven by the longwave feedback component (Fig. B2a), and reflects that larger Antarctic sea ice loss is systematically linked to stronger high-latitude warming and more negative local Planck feedback across ESMs (Fig. B2c,d).

In sum, across ESMs, stronger Antarctic sea ice loss links to larger net feedback both locally, through a more positive surface albedo feedback, and remotely, by systematically projecting onto cloud feedbacks beyond high latitudes. While the local albedo response is readily understood, interpreting the link between Southern Ocean variability and remote cloud feedbacks is more complex.

Cloud feedback remains a major source of uncertainty in climate sensitivity estimates, with much of its spread arising from the shortwave component [8]. Previous

work has shown that clouds, particularly marine low clouds, are highly sensitive to patterns of SST warming [7, 15, 16, 26, 27], and that their radiative response to surface warming is a key driver of model uncertainty in long-term cloud feedback estimates [28–32]. More broadly, the inter-model spread in net feedback is primarily owed to model differences in SST warming patterns in equilibrium climate responses [28]. We therefore argue that quantifying how differently coupled ESMs project SST warming patterns provides a crucial piece for understanding the physical link between Southern Ocean variability and hemispheric cloud feedbacks.

Model differences in SST pattern link Southern Ocean sea ice to remote cloud feedbacks

To quantify differences in SST warming patterns across ESMs, we perform an inter-model empirical orthogonal function (EOF) analysis on fields of local SST changes normalized by global mean temperature change $\Delta\text{SST}/\Delta\overline{T}$. As such, the EOF decomposition isolates the dominant modes of inter-model disagreement in SST pattern response as a single scalar metric, which can be directly linked to Southern Ocean variability.

We focus on the three leading modes of inter-model variability in $\Delta\text{SST}/\Delta\overline{T}$, which together explain the majority of model variance. The leading mode alone accounts for 31.7% of the variance (Fig. C3). The corresponding principal component (PC1) exhibits a robust correlation with Antarctic sea ice loss, whereas no meaningful relationship is found for PC2 and PC3. As such, Antarctic sea ice loss aligns closely with the primary axis of inter-model variability in SST warming pattern.

Regressing PC1 onto feedback fields reveals spatially coherent patterns across the Southern Hemisphere (Fig. 3). Since larger Antarctic sea ice loss is associated with positive PC1 scores (Fig. C3), positive regression values in Fig. 3 correspond to SST and feedback anomalies characteristic of models with stronger sea ice loss. For clarity, we hereafter refer to positive regression values as increases or positive anomalies relative to the multi-model mean, and vice versa.

Over the Southern Ocean south of 60°S, models with stronger ice loss systematically show positive SST and surface albedo feedback anomalies (Fig. 3a,d). The positive SST pattern anomalies extend northward into the Southern mid-latitudes around 40–60°S, and spatially coincide with positive shortwave cloud feedback anomalies with widespread statistical robustness (Fig. 3a,c). Positive SST anomalies extend further northward in the Pacific basin, with warm anomalies reaching the equatorial eastern Pacific in conjunction with more positive shortwave cloud feedbacks. Taken together, these SST-feedback couplings shape a coherent positive anomaly in net shortwave feedback throughout the Southern Hemisphere (Fig. 3b).

The SST pattern that emerges from our inter-model EOF analysis (Fig. 3a) is reminiscent of previous work that perturbed Southern Ocean climate in atmosphere-only simulations, and in which SST anomalies propagate northward, zonally homogenized across the Southern storm-track region, and extended into the equatorial Pacific [12, 13]. In these studies, emerging patterns have been interpreted as signatures of

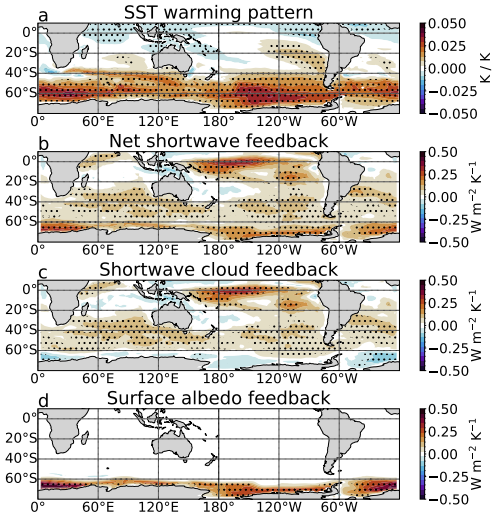


Fig. 3 Feedback anomalies associated with the leading mode of inter-model variability in SST warming pattern. An inter-model EOF analysis was performed on SST warming patterns across CMIP6 models. The leading PC1 score correlates strongly with Antarctic sea ice loss, and is regressed onto fields of SST pattern itself and shortwave feedbacks. In the EOF analysis, models with the strongest Antarctic sea ice loss give a positive PC1 score close to 1 (Fig. C3), and more closely resemble patterns as in panels (a)–(d). Black dots indicate regions where regressions are statistically significant at the 95% confidence level.

a Southern Ocean–tropical Pacific teleconnection pathway driven, among other factors, by anomalous atmospheric stability, climatological winds, cloud cover, and ocean upwelling [12, 13].

We find fingerprints of these teleconnection pathways by regressing PC1 score onto a suite of relevant dynamical and thermodynamical diagnostics (Fig. C4). The coherent positive SST anomaly around 40–60°S coincides with reduced baroclinicity, weaker near-surface winds with anomalous north-westerly flow, decreased estimated inversion strength (EIS) and large-scale reductions in cloud fraction (Fig. C4a–d, respectively), with widespread statistical significance. The "warm tongue" of positive SST anomalies reaching into the eastern Pacific basin is mostly associated with lower wind speeds and anomalous south-easterly flow, regions of weakened upwelling, reduced EIS, and a particularly large and significant cloud fraction decrease in the eastern equatorial Pacific (Fig. C4). Particularly the strong local cloud responses was previously isolated as key driver of global feedback anomalies in response to Southern Ocean variability in the historical period [13]. Here, a similar structure emerges spontaneously as the dominant axis of SST response variability across an ensemble of freely evolving ESMs, with strong ties to Antarctic sea ice.

Emergent constraint on climate sensitivity: Implications of recent Antarctic sea ice decline

Our results to this point suggest that inter-model differences in pre-industrial Antarctic SIA partly set the stage for the coupled evolution of sea ice loss and Southern Ocean

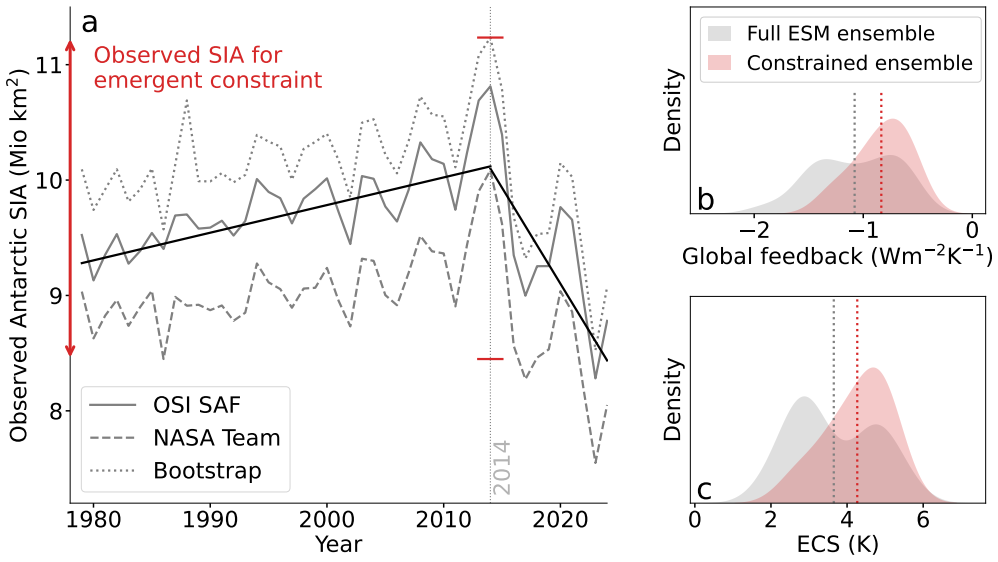


Fig. 4 Process-oriented emergent constraint on climate sensitivity based on Antarctic SIA in CMIP6. (a) Observed Antarctic SIA from three satellite products (OSI SAF, NASA Team, Bootstrap; gray lines), and their mean positive trend over 1979–2014 followed by a negative trend after 2014 (black lines). Red arrow: Observational range used to constrain the ESM ensemble, derived as minimum to maximum annual value over 1979–2014 and three data records. (b) Distribution of global feedback across all ESMs (gray) and constrained ESM subset (red). Vertical dotted lines indicate ensemble means. (c) Same as (b) but for ECS. The emergent constraint is based on the linear relationship between *piControl* SIA and global feedback in Fig. 1e. The constraint reduces the ECS very likely (90%) range from 2.4–5.1 K to 3.3–5.0 K.

warming, hemispheric SST patterns, and long-term feedbacks under CO_2 forcing. Based on our robust and physically grounded relationships across ESMs, we construct a process-oriented emergent constraint using satellite observations of Antarctic SIA from 1979 onward.

We justify the comparison between pre-industrial SIA in ESMs and satellite-era observations by noting that observed Antarctic SIA remained relatively stable over the period 1979–2014, exhibiting weak positive trends and reaching a record maximum in 2014 (Fig. 4a). This expansion phase was followed by a rapid decline—now marking a full decade of anomalously low SIA [23]—and was potentially driven by unusual atmospheric conditions [33, 34] and subsurface ocean warming [35]. This unprecedented decline in Antarctic sea ice has further raised the prospect of a lasting regime shift in the coupled Southern Ocean climate system [22, 35–37]. We therefore base our emergent constraint on the 1979–2014 period, treating it as a quasi-stationary baseline prior to the decline phase.

Applying the emergent constraint method narrows the ESM ensemble and shifts the distribution toward higher global feedback and ECS values (Fig. 4b,c). The constraint yields a very likely (90%) ECS range of 3.3–5.0 K, placing our estimate toward the upper end of the latest IPCC AR6 estimate of 2.0–5.0 K. This upward shift is consistent

with on average higher ECS values in CMIP6 relative to the IPCC AR6 best estimate. It also coincides with on average higher ECS in CMIP6 compared to CMIP5, including the emergence of several high-sensitivity models exceeding the upper range of CMIP5 [8]. Two of these models, CESM2 and CNRM-CM6-1, fall within our constrained ensemble. The emergence of high-sensitivity models has to some extent been associated with changes in mixed-phase cloud processes over the Southern Ocean between model generations. In particular, an increase in mean-state cloud liquid water fraction has led to weaker increases in both cloud abundance and albedo under forcing, corresponding to a less negative shortwave cloud feedback over the Southern Ocean [8]. At the same time, an increased mean-state cloud liquid water fraction in some high-sensitivity models may have also reduced concurrent warm-SST and low-SIA biases over the Southern Ocean [11], making those models more realistic in their representation of Antarctic SIA in the scope of our emergent constraint.

These atmosphere–ocean–sea-ice couplings also highlight that Antarctic SIA is not the sole possible metric to characterize the Southern Ocean mean state. Rather, we employ Antarctic SIA as an observable proxy for the underlying coupled Southern Ocean climate system prior to external forcing. Nevertheless, our estimate should still not be over-interpreted quantitatively, given that it relies on comparing simulated pre-industrial SIA with satellite-era observations. Moreover, while previous ECS assessment studies integrate multiple independent lines of evidence [38], our approach represents a process-oriented emergent constraint, which may itself be subject to biases [39].

Instead, our results suggest that the present-day Southern Ocean climate system, characterized by relatively extensive SIA compared to ESMs, is predisposed toward an equilibrium response involving more sea ice loss, stronger Southern Ocean warming, and larger hemispheric feedbacks compared to the majority of ESMs. The recent decline in Antarctic SIA may therefore signal the emergence of such a regime, with implications for larger ECS than previously assumed. We motivate future research aimed at investigating the direct role of the past decade's unprecedented Southern Ocean sea ice melt and warming in driving positive feedback anomalies with global-scale impact.

Methods

CMIP6 data

We considered the full CMIP6 archive, from which 25 ESMs provided all required diagnostics for our emergent constraint: ACCESS-CM2, CESM2, CESM2-FV2, CESM2-WACCM, CESM2-WACCM-FV2, CMCC-CM2-SR5, CNRM-CM6-1, CNRM-CM6-1-HR, CNRM-ESM2-1, CanESM5, GFDL-CM4, GFDL-ESM4, GISS-E2-1-H, HadGEM3-GC31-MM, INM-CM4-8, INM-CM5-0, IPSL-CM6A-LR, MIROC-ES2L, MIROC6, MPI-ESM-1-2-HAM, MPI-ESM1-2-HR, MPI-ESM1-2-LR, MRI-ESM2-0, NorESM2-MM, SAM0-UNICON. We used the first realization of each model's pre-industrial control (*piControl*) and CO_2-quadrupling experiment (*abrupt4xCO2*). Changes in all variables were derived from the the linear regression slope of the 150-year time series of differences between *abrupt4xCO2* and *piControl*

simulations. All results were derived from monthly output. Inter-model relationships were assessed using linear regression.

Climate sensitivity and feedbacks

The global feedback parameter and ECS were estimated using the Gregory regression method [5]. For each model, annual-mean global top-of-atmosphere radiative imbalance N was regressed against annual-mean global surface air temperature anomaly $\Delta\overline{T}$ over the course of 150 years of *abrupt4xCO2* minus *piControl* time series: $N = F - \lambda\Delta\overline{T}$. F is the effective radiative forcing (intercept at $\Delta\overline{T} = 0$), and λ is the global feedback parameter (regression slope). ECS was estimated as $\mathrm{ECS} = \frac{1}{2}F/\lambda$, giving the near-equilibrium warming at $N \approx 0$ following a doubling of CO_2.

To break down the net feedback into components resulting from changes in temperature, surface albedo, water vapour and clouds, we applied the radiative kernel method [40, 41]. Feedbacks are given as averages from 11 radiative kernels derived from different radiation schemes: BMRC [40], CAM3 [42], CAM5 [43], CERES [44], CloudSat [45], ECHAM6 [46], ECMWF-RRTM [47], ERA5 [48], GFDL [1], HadGEM2 [49], and HadGEM3-GA7.1 [50].

Inter-model EOF analysis

To link Southern Ocean variability to remote cloud feedbacks, we performed an inter-model EOF analysis on Southern-Hemisphere patterns of SST warming. We focused on the leading mode, which represents the primary axis of inter-model variability. We then regressed the PC1 score onto hemispheric feedback fields.

To further elaborate on physical mechanisms, we extended the regression framework to a suite of dynamical and thermodynamical diagnostics. We considered the maximum Eady growth rate (EGR) at 700 hPa pressure level, near-surface (10 m) winds, estimated inversion strength (EIS), cloud fraction, and surface wind stress curl. The maximum EGR is a measure for baroclinic instability, and was derived as $\sigma = 0.31\,\frac{f}{N}\left|\frac{\partial u}{\partial z}\right|$, where f is the Coriolis parameter, N is the Brunt–Väisälä frequency, and $\partial u/\partial z$ is the vertical shear of the zonal wind [51, 52]. EIS characterizes lower-tropospheric stability relevant for low-cloud formation, and was computed as $\mathrm{EIS} = \theta_{700} - \theta_{\mathrm{surface}} - \Gamma_m^{850}\,(z_{700} - z_{\mathrm{LCL}})$, where θ_{700} and $\theta_{\mathrm{surface}}$ are the potential temperatures at 700 hPa and the surface, Γ_m^{850} is the moist adiabatic lapse rate at 850 hPa, z_{700} is the height of the 700 hPa level, and z_{LCL} is the lifting condensation level [53, 54]. The wind stress curl is directly related to ocean Ekman pumping, and was computed as the vertical component of the curl of the surface wind stress vector, $\nabla \times \boldsymbol{\tau} = \frac{\partial \tau_y}{\partial x} - \frac{\partial \tau_x}{\partial y}$ where $\boldsymbol{\tau} = (\tau_x, \tau_y)$ is the zonal and meridional surface wind stress.

Sea ice area in models and observations

Model-based SIA was computed on native grids as the area integral of monthly sea ice concentration (SIC) over the ocean surface of the respective hemisphere. We prefer SIA as estimate over sea ice extent (SIE) as it accounts for subgrid-scale variability in ice cover, while SIE applies a fixed SIC threshold of 15% [23, 55]. SIA further

avoids artificial sensitivity to SIC threshold choices, and allows direct comparisons to previous work on Antarctic sea ice in CMIP6 [21, 23].

SIA from satellite observations was computed from daily SIC on native grid and averaged over each year. Following previous recommendations [21, 23], we considered sample uncertainty by using different observational products: OSI SAF [56], NASA-Team [57], and Bootstrap [58].

Data availability

All CMIP6 data is publicly available via the Earth System Grid Federation (ESGF; https://esgf-node.llnl.gov/search/cmip6/) and was accessed through the German Climate Computing Centre (DKRZ) and ESMValTool [59]. SIC data from satellite was downloaded from the Copernicus Climate Data Store for OSI SAF (https://doi.org/10.24381/cds.3cd8b812), and from the National Snow and Ice Data Center for NASA Team (https://doi.org/10.5067/MPYG15WAA4WX) and Bootstrap algorithms (https://doi.org/10.5067/X5LG68MH013O).

Code availability

The code relating to this study is available from the corresponding author on request.

Acknowledgements. The study was supported by the Knut and Alice Wallenberg foundation under grant no. 2023.0253 (ACCELERATE). We acknowledge the World Climate Research Programme which coordinated and promoted CMIP6. We thank the climate modelling groups for producing and making available their model output, the Earth System Grid Federation (ESGF) for archiving the data and providing access, and the multiple funding agencies who support CMIP6 and ESGF.

Appendix A Northern Hemisphere SIA and global feedback

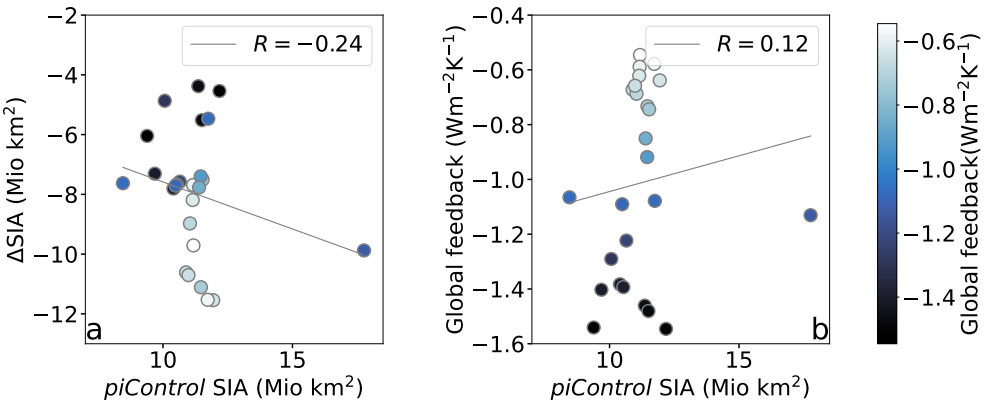


Fig. A1 Links between Arctic sea ice and global feedback across CMIP6 models. Inter-model relationships between (a) *piControl* Arctic SIA and sea ice loss ΔSIA, and (b) *piControl* Arctic SIA and global feedback.

Appendix B Zonal longwave feedbacks and links to Antarctic SIA

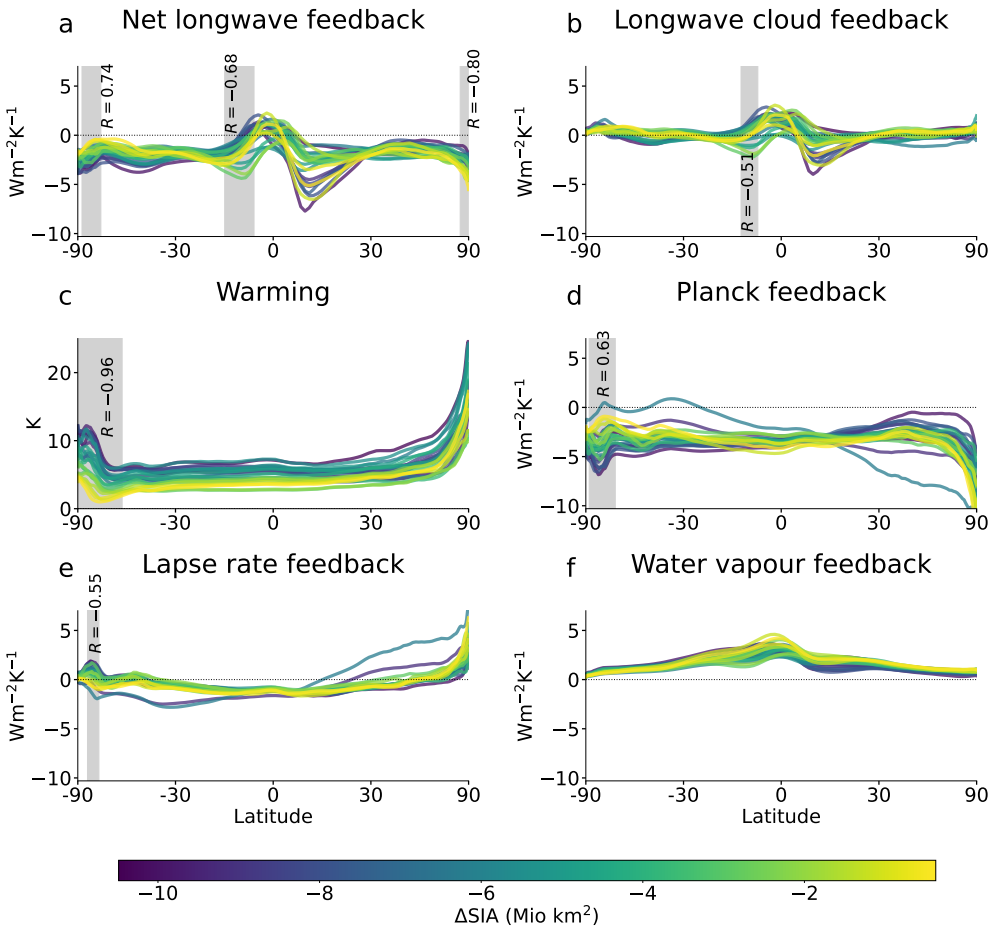


Fig. B2 Links between Antarctic sea ice loss and longwave zonal feedbacks across CMIP6 models. As Fig. 2, but with zonal-mean profiles showing longwave feedbacks and warming of individual ESMs, colour-coded by the magnitude of Antarctic sea ice loss ΔSIA.

Appendix C Inter-model EOF analysis on SST warming patterns

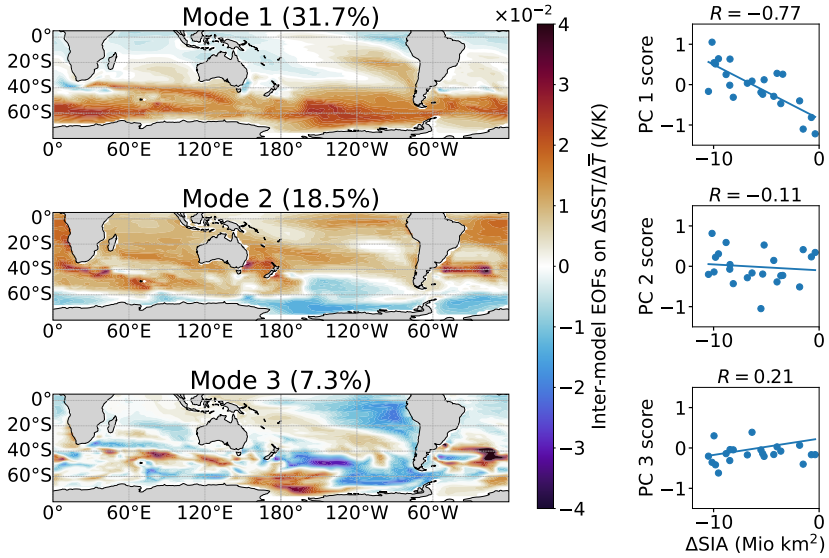


Fig. C3 Inter-model empirical orthogonal function (EOF) analysis on SST warming pattern across CMIP6 models. Left column: The three leading EOFs on $\Delta\mathrm{SST}/\Delta\overline{T}$, representing the dominant modes of inter-model SST pattern variability. Numbers indicate the fraction of inter-model variance explained by each mode. Right: Relationship between the principal component (PC) scores and Antarctic sea ice loss across ESMs.

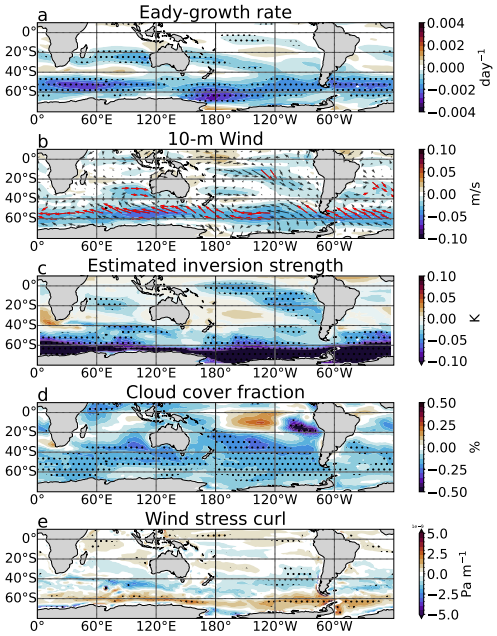


Fig. C4 Anomalies associated with the leading mode of inter-model variability in SST warming pattern. As Fig. 3, but with PC1 score regressed onto (a) the Eady-growth rate (EGR) at 700 hPa pressure level as proxy for baroclinic stability, (b) 10-m wind speed and vector, with red vectors indicating statistical significance, (c) the estimated inversion strength (EIS), (d) the total cloud fraction, and (e) the wind stress curl with positive values indicating upwelling.

References

[1] Soden, B.J., Held, I.M.: An assessment of climate feedbacks in coupled ocean-atmosphere models. J. Clim. **19**(14), 3354–3360 (2006) https://doi.org/10.1175/JCLI3799.1

[2] Bony, S., Colman, R., Kattsov, V.M., Allan, R.P., Bretherton, C.S., Dufresne, J.-L., Hall, A., Hallegatte, S., Holland, M.M., Ingram, W., *et al.*: How well do we understand and evaluate climate change feedback processes? Journal of Climate **19**(15), 3445–3482 (2006) https://doi.org/10.1175/JCLI3819.1

[3] Andrews, T., Gregory, J.M., Webb, M.J., Taylor, K.E.: Forcing, feedbacks and climate sensitivity in CMIP5 coupled atmosphere-ocean climate models. Geophysical research letters **39**(9) (2012) https://doi.org/10.1029/2012GL051607

[4] Knutti, R., Rugenstein, M.A., Hegerl, G.C.: Beyond equilibrium climate sensitivity. Nature Geoscience **10**(10), 727–736 (2017) https://doi.org/10.1038/ngeo3017

[5] Gregory, J.M., Ingram, W.J., Palmer, M., Jones, G.S., Stott, P., Thorpe, R., Lowe, J.A., Johns, T., Williams, K.: A new method for diagnosing radiative forcing and

climate sensitivity. Geophysical research letters **31**(3) (2004) https://doi.org/10.1029/2003GL018747

[6] Armour, K.C., Bitz, C.M., Roe, G.H.: Time-varying climate sensitivity from regional feedbacks. Journal of Climate **26**(13), 4518–4534 (2013) https://doi.org/10.1175/JCLI-D-12-00544.1

[7] Ceppi, P., Gregory, J.M.: Relationship of tropospheric stability to climate sensitivity and Earth's observed radiation budget. Proceedings of the National Academy of Sciences **114**(50), 13126–13131 (2017) https://doi.org/10.1073/pnas.1714308114

[8] Zelinka, M.D., Myers, T.A., McCoy, D.T., Po-Chedley, S., Caldwell, P.M., Ceppi, P., Klein, S.A., Taylor, K.E.: Causes of higher climate sensitivity in CMIP6 models. Geophysical Research Letters **47**(1), 2019–085782 (2020) https://doi.org/10.1029/2019GL085782

[9] Rugenstein, M., Bloch-Johnson, J., Gregory, J., Andrews, T., Mauritsen, T., Li, C., Frölicher, T.L., Paynter, D., Danabasoglu, G., Yang, S., *et al.*: Equilibrium climate sensitivity estimated by equilibrating climate models. Geophysical Research Letters **47**(4), 2019–083898 (2020) https://doi.org/10.1029/2019GL083898

[10] Meehl, G.A., Senior, C.A., Eyring, V., Flato, G., Lamarque, J.-F., Stouffer, R.J., Taylor, K.E., Schlund, M.: Context for interpreting equilibrium climate sensitivity and transient climate response from the CMIP6 Earth system models. Science Advances **6**(26), 1981 (2020) https://doi.org/10.1126/sciadv.aba1981

[11] Flynn, C.M., Mauritsen, T.: On the climate sensitivity and historical warming evolution in recent coupled model ensembles. Atmospheric Chemistry and Physics **20**(13), 7829–7842 (2020) https://doi.org/10.5194/acp-20-7829-2020

[12] Kim, H., Kang, S.M., Kay, J.E., Xie, S.-P.: Subtropical clouds key to Southern Ocean teleconnections to the tropical Pacific. Proceedings of the National Academy of Sciences **119**(34), 2200514119 (2022) https://doi.org/10.1073/pnas.2200514119

[13] Kang, S.M., Ceppi, P., Yu, Y., Kang, I.-S.: Recent global climate feedback controlled by Southern Ocean cooling. Nature Geoscience **16**(9), 775–780 (2023) https://doi.org/10.1038/s41561-023-01256-6

[14] Zhou, C., Zelinka, M.D., Klein, S.A.: Impact of decadal cloud variations on the Earth's energy budget. Nature Geoscience **9**(12), 871–874 (2016) https://doi.org/10.1038/ngeo2828

[15] Dong, Y., Proistosescu, C., Armour, K.C., Battisti, D.S.: Attributing historical and future evolution of radiative feedbacks to regional warming patterns using a Green's function approach: The preeminence of the western Pacific. Journal of

Climate **32**(17), 5471–5491 (2019) https://doi.org/10.1175/JCLI-D-18-0843.1

[16] Andrews, T., Bodas-Salcedo, A., Gregory, J.M., Dong, Y., Armour, K.C., Paynter, D., Lin, P., Modak, A., Mauritsen, T., Cole, J.N., *et al.*: On the effect of historical SST patterns on radiative feedback. Journal of Geophysical Research: Atmospheres **127**(18), 2022–036675 (2022) https://doi.org/10.1029/2022JD036675

[17] Wills, R.C., Dong, Y., Proistosecu, C., Armour, K.C., Battisti, D.S.: Systematic climate model biases in the large-scale patterns of recent sea-surface temperature and sea-level pressure change. Geophysical Research Letters **49**(17), 2022–100011 (2022) https://doi.org/10.1029/2022GL100011

[18] Meehl, G.A., Arblaster, J.M., Bitz, C.M., Chung, C.T., Teng, H.: Antarctic sea-ice expansion between 2000 and 2014 driven by tropical Pacific decadal climate variability. Nature Geoscience **9**(8), 590–595 (2016) https://doi.org/10.1038/ngeo2751

[19] Chung, E.-S., Kim, S.-J., Timmermann, A., Ha, K.-J., Lee, S.-K., Stuecker, M.F., Rodgers, K.B., Lee, S.-S., Huang, L.: Antarctic sea-ice expansion and Southern Ocean cooling linked to tropical variability. Nature Climate Change **12**(5), 461–468 (2022) https://doi.org/10.1038/s41558-022-01339-z

[20] Kang, S.M., Yu, Y., Deser, C., Zhang, X., Kang, I.-S., Lee, S.-S., Rodgers, K.B., Ceppi, P.: Global impacts of recent Southern Ocean cooling. Proceedings of the National Academy of Sciences **120**(30), 2300881120 (2023) https://doi.org/10.1073/pnas.2300881120

[21] Roach, L.A., Dörr, J., Holmes, C.R., Massonnet, F., Blockley, E.W., Notz, D., Rackow, T., Raphael, M.N., O'Farrell, S.P., Bailey, D.A., *et al.*: Antarctic sea ice area in CMIP6. Geophysical Research Letters **47**(9), 2019–086729 (2020) https://doi.org/10.1029/2019GL086729

[22] Eayrs, C., Li, X., Raphael, M.N., Holland, D.M.: Rapid decline in Antarctic sea ice in recent years hints at future change. Nature Geoscience **14**(7), 460–464 (2021) https://doi.org/10.1038/s41561-021-00768-3

[23] Roach, L.A., Polvani, L.M.: Persistent Antarctic sea ice biases in CMIP6 models in spite of the recent decade-long sharp decline. Journal of Climate, 250477 (2026) https://doi.org/10.1175/JCLI-D-25-0477.1

[24] Luo, F., Ying, J., Liu, T., Chen, D.: Origins of Southern Ocean warm sea surface temperature bias in CMIP6 models. npj Climate and Atmospheric Science **6**(1), 127 (2023) https://doi.org/10.1038/s41612-023-00456-6

[25] Song, Z., Jing, Z., Yuan, M., Li, Z., Wang, H., Song, F., Yang, H., Du, T., Wu, L.: Reduced warm bias in the surface Southern Ocean by improved parameterization of wind-driven vertical mixing in an eddy-resolving coupled global

climate model. Geophysical Research Letters **52**(18), 2025–115504 (2025) https://doi.org/10.1029/2025GL115504

[26] Zhou, C., Zelinka, M.D., Klein, S.A.: Analyzing the dependence of global cloud feedback on the spatial pattern of sea surface temperature change with a G reen's function approach. Journal of Advances in Modeling Earth Systems **9**(5), 2174–2189 (2017) https://doi.org/10.1002/2017MS001096

[27] Andrews, T., Webb, M.J.: The dependence of global cloud and lapse rate feedbacks on the spatial structure of tropical Pacific warming. Journal of Climate **31**(2), 641–654 (2018) https://doi.org/10.1175/JCLI-D-17-0087.1

[28] Dong, Y., Armour, K.C., Zelinka, M.D., Proistosescu, C., Battisti, D.S., Zhou, C., Andrews, T.: Intermodel spread in the pattern effect and its contribution to climate sensitivity in CMIP5 and CMIP6 models. Journal of Climate **33**(18), 7755–7775 (2020) https://doi.org/10.1175/JCLI-D-19-1011.1

[29] Ceppi, P., Nowack, P.: Observational evidence that cloud feedback amplifies global warming. Proceedings of the National Academy of Sciences **118**(30), 2026290118 (2021) https://doi.org/10.1073/pnas.2026290118

[30] Myers, T.A., Norris, J.R.: Reducing the uncertainty in subtropical cloud feedback. Geophysical Research Letters **43**(5), 2144–2148 (2016) https://doi.org/10.1002/2015GL067416

[31] Qu, X., Hall, A., Klein, S.A., Caldwell, P.M.: On the spread of changes in marine low cloud cover in climate model simulations of the 21st century. Climate dynamics **42**(9), 2603–2626 (2014) https://doi.org/10.1007/s00382-013-1945-z

[32] Kawaguchi, K., Ceppi, P.: Responses to lower-tropospheric stability dominate intermodel differences in the historical pattern effect. Geophysical Research Letters **52**(17), 2025–117015 (2025) https://doi.org/10.1029/2025GL117015

[33] Wilson, E.A., Bonan, D.B., Thompson, A.F., Armstrong, N., Riser, S.C.: Mechanisms for abrupt summertime circumpolar surface warming in the Southern Ocean. Journal of Climate **36**(20), 7025–7039 (2023) https://doi.org/10.1175/JCLI-D-22-0501.1

[34] Purich, A., England, M.H.: Tropical teleconnections to Antarctic sea ice during austral spring 2016 in coupled pacemaker experiments. Geophysical Research Letters **46**(12), 6848–6858 (2019) https://doi.org/10.1029/2019GL082671

[35] Purich, A., Doddridge, E.W.: Record low Antarctic sea ice coverage indicates a new sea ice state. Communications Earth & Environment **4**(1), 314 (2023) https://doi.org/10.1038/s43247-023-00961-9

[36] Raphael, M.N., Handcock, M.S.: A new record minimum for Antarctic sea ice.

Nature Reviews Earth & Environment **3**(4), 215–216 (2022) https://doi.org/10.1038/s43017-022-00281-0

[37] Hobbs, W., Spence, P., Meyer, A., Schroeter, S., Fraser, A.D., Reid, P., Tian, T.R., Wang, Z., Liniger, G., Doddridge, E.W., *et al.*: Observational evidence for a regime shift in summer Antarctic sea ice. Journal of Climate **37**(7), 2263–2275 (2024) https://doi.org/10.1175/JCLI-D-23-0479.1

[38] Sherwood, S.C., Webb, M.J., Annan, J.D., Armour, K.C., Forster, P.M., Hargreaves, J.C., Hegerl, G., Klein, S.A., Marvel, K.D., Rohling, E.J., *et al.*: An assessment of Earth's climate sensitivity using multiple lines of evidence. Reviews of geophysics **58**(4), 2019–000678 (2020) https://doi.org/10.1029/2019RG000678

[39] Schlund, M., Lauer, A., Gentine, P., Sherwood, S.C., Eyring, V.: Emergent constraints on equilibrium climate sensitivity in CMIP5: do they hold for CMIP6? Earth System Dynamics **11**(4), 1233–1258 (2020) https://doi.org/10.5194/esd-11-1233-2020

[40] Soden, B.J., Held, I.M., Colman, R., Shell, K.M., Kiehl, J.T., Shields, C.A.: Quantifying climate feedbacks using radiative kernels. Journal of Climate **21**(14), 3504–3520 (2008) https://doi.org/10.1175/2007JCLI2110.1

[41] Janoski, T.P., Mitevski, I., Kramer, R.J., Previdi, M., Polvani, L.M.: ClimKern v1. 2: a new Python package and kernel repository for calculating radiative feedbacks. Geoscientific Model Development **18**(10), 3065–3079 (2025) https://doi.org/10.5194/gmd-18-3065-2025

[42] Shell, K.M., Kiehl, J.T., Shields, C.A.: Using the radiative kernel technique to calculate climate feedbacks in NCAR's Community Atmospheric Model. Journal of Climate **21**(10), 2269–2282 (2008) https://doi.org/10.1175/2007JCLI2044.1

[43] Pendergrass, A.G., Conley, A., Vitt, F.M.: Surface and top-of-atmosphere radiative feedback kernels for CESM-CAM5. Earth System Science Data **10**(1), 317–324 (2018) https://doi.org/10.5194/essd-10-317-2018

[44] Thorsen, T.J., Kato, S., Loeb, N.G., Rose, F.G.: Observation-based decomposition of radiative perturbations and radiative kernels. Journal of climate **31**(24), 10039–10058 (2018) https://doi.org/10.1175/JCLI-D-18-0045.1

[45] Kramer, R.J., Matus, A.V., Soden, B.J., L'Ecuyer, T.S.: Observation-based radiative kernels from CloudSat/CALIPSO. Journal of Geophysical Research: Atmospheres **124**(10), 5431–5444 (2019) https://doi.org/10.1029/2018JD029021

[46] Block, K., Mauritsen, T.: Forcing and feedback in the MPI-ESM-LR coupled model under abruptly quadrupled CO2. Journal of Advances in Modeling Earth Systems **5**(4), 676–691 (2013) https://doi.org/10.1002/jame.20041

[47] Huang, Y., Xia, Y., Tan, X.: On the pattern of CO2 radiative forcing and poleward energy transport. Journal of Geophysical Research: Atmospheres **122**(20), 10–578 (2017) https://doi.org/10.1002/2017JD027221

[48] Huang, H., Huang, Y.: Radiative sensitivity quantified by a new set of radiation flux kernels based on the ECMWF Reanalysis v5 (ERA5). Earth System Science Data **15**(7), 3001–3021 (2023) https://doi.org/10.5194/essd-15-3001-2023

[49] Smith, C., Kramer, R., Myhre, G., Forster, P., Soden, B., Andrews, T., Boucher, O., Faluvegi, G., Fläschner, D., Hodnebrog, Ø., *et al.*: Understanding rapid adjustments to diverse forcing agents. Geophysical Research Letters **45**(21), 12–023 (2018) https://doi.org/10.1029/2018GL079826

[50] Smith, C.J., Kramer, R.J., Sima, A.: The HadGEM3-GA7. 1 radiative kernel: the importance of a well-resolved stratosphere. Earth System Science Data **12**(3), 2157–2168 (2020) https://doi.org/10.5194/essd-12-2157-2020

[51] Moreno-Chamarro, E., Caron, L.-P., Ortega, P., Loosveldt Tomas, S., Roberts, M.J.: Can we trust CMIP5/6 future projections of European winter precipitation? Environmental Research Letters **16**(5), 054063 (2021) https://doi.org/10.1088/1748-9326/abf28a

[52] Hoskins, B.J., Valdes, P.J.: On the existence of storm-tracks. Journal of Atmospheric Sciences **47**(15), 1854–1864 (1990) https://doi.org/10.1175/1520-0469(1990)047⟨1854:OTEOST⟩2.0.CO;2

[53] Cutler, L., Brunke, M.A., Zeng, X.: Re-evaluation of low cloud amount relationships with lower-tropospheric stability and estimated inversion strength. Geophysical Research Letters **49**(12), 2022–098137 (2022) https://doi.org/10.1029/2022GL098137

[54] Wood, R., Bretherton, C.S.: On the relationship between stratiform low cloud cover and lower-tropospheric stability. Journal of climate **19**(24), 6425–6432 (2006) https://doi.org/10.1175/JCLI3988.1

[55] Notz, D., SIMIP Community: Arctic Sea Ice in CMIP6. Geophysical Research Letters **47**(10), 2019–086749 (2020) https://doi.org/10.1029/2019GL086749

[56] Lavergne, T., Sørensen, A.M., Kern, S., Tonboe, R., Notz, D., Aaboe, S., Bell, L., Dybkjær, G., Eastwood, S., Gabarro, C., Heygster, G., Killie, M.A., Brandt Kreiner, M., Lavelle, J., Saldo, R., Sandven, S., Pedersen, L.T.: Version 2 of the EUMETSAT OSI SAF and ESA CCI sea-ice concentration climate data records. The Cryosphere **13**(1), 49–78 (2019) https://doi.org/10.5194/tc-13-49-2019

[57] DiGirolamo, N.E., Parkinson, C.L., Cavalieri, D.J., Gloersen, P., Zwally, H.J.: Sea Ice Concentrations from Nimbus-7 SMMR and DMSP SSM/I-SSMIS Passive Microwave Data, Version 2. https://doi.org/10.5067/MPYG15WAA4WX . [Data

set id: NSIDC-0051]

[58] Comiso, J.C., Gersten, R.A.: Bootstrap Sea Ice Concentrations from Nimbus-7 SMMR and DMSP SSM/I-SSMIS, Version 4. https://doi.org/10.5067/X5LG68MH013O . [Data set id: NSIDC-0079]

[59] Lauer, A., Bock, L., Hassler, B., Jöckel, P., Ruhe, L., Schlund, M.: Monitoring and benchmarking Earth system model simulations with ESMValTool v2. 12.0. Geoscientific Model Development **18**(4), 1169–1188 (2025) https://doi.org/10.5194/gmd-18-1169-2025